Supporting Information

Comparison of Solid-State Dipolar Couplings and Solution Relaxation Data Provides Insight into Protein Backbone Dynamics.

Veniamin Chevelkov,[†‡] Yi Xue,[‡] Rasmus Linser,[†] Nikolai R. Skrynnikov,[‡]*Bernd Reif[†]*

† *Forschunginstitut für Molekulare Pharmakologie (FMP), Robert-Rössle-Strasse 10, 13125 Berlin, Germany*

‡ *Department of Chemistry, Purdue University, 560 Oval Drive, W. Lafayette, Indiana 47907-2084*

nikolai@purdue.edu; reif@fmp-berlin.de

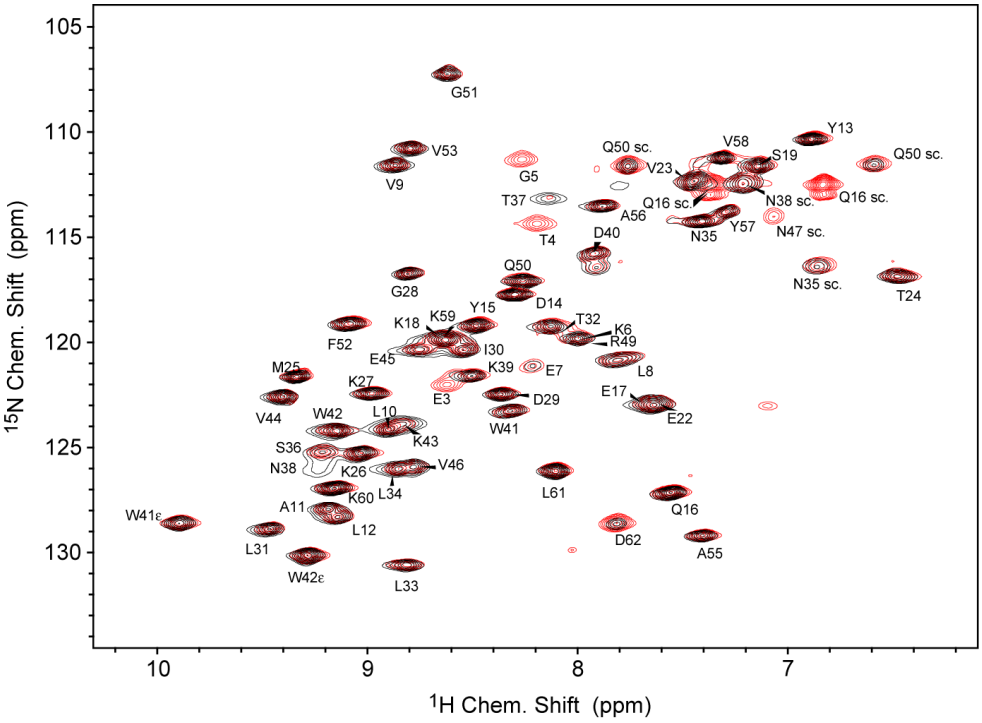

Figure S1. Two superimposed solid-state spectra of α-spectrin SH3 domain. Recorded by means of HSQC-style pulse sequences employing INEPT transfer elements (red contour lines) or, alternatively, CP transfer elements (black contour lines). Special effort has been made to acquire the data under identical conditions: $t_1^{max} = 93$ ms (400 increments, scalar coupling refocused using ^{1}H 180º composite pulse), $t_2^{max} = 80$ ms (WALTZ-16 ^{15}N decoupling, 2.5 kHz *rf* field strength), measurement time 2.5 h per spectrum. The spectra were recorded back-to-back using the protein sample with 25% content of back-exchanged protons, doped with 75 mM Cu-EDTA[1] at static magnetic field strength 600 MHz, MAS speed 24 kHz, temperature 22 ºC. Processing and plotting parameters for the two spectra are identical.

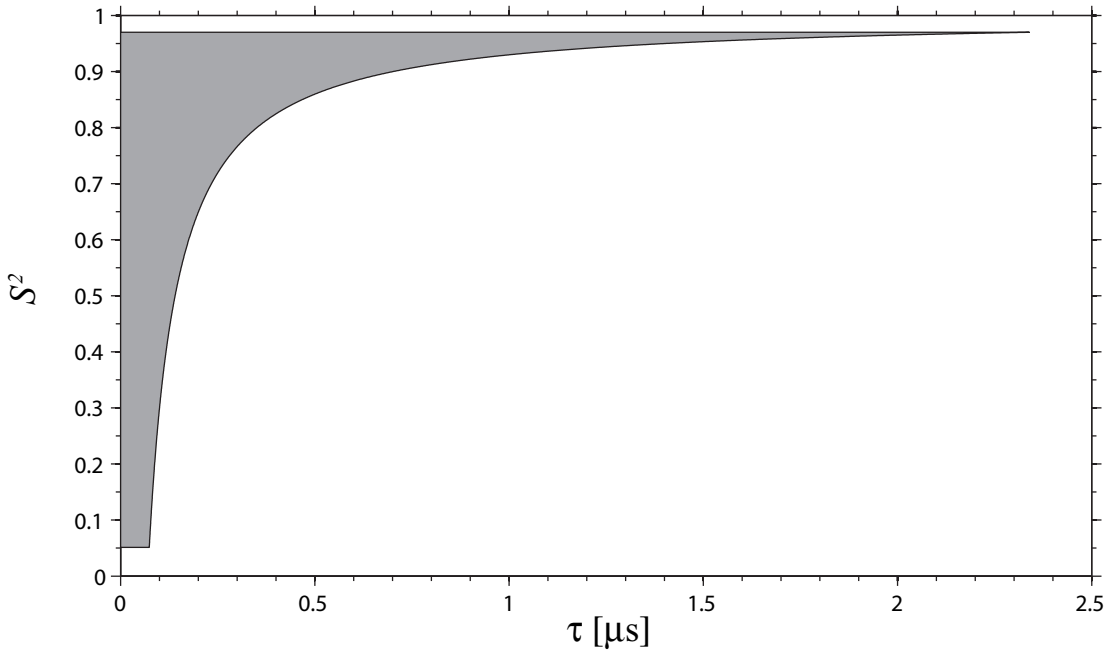

Figure S2. Range of dynamic parameters $\{S^2, \tau\}$ that can be probed by means of solid-state DC measurements (shaded area in the plot). The area is constrained by: (*i*) $S^2 = 0.97$ (at the current level of accuracy, higher S^2 values cannot be distinguished from 1.0), (*ii*) $S^2 = 0.05$ (lower S^2 values produce small DC constants that cannot be properly sampled using the current experimental scheme[2]), and (*iii*) the curve corresponding to $R_2 = 100$ s^{-1} (it is assumed that higher relaxation rates cause excessive line broadening). The above choice of boundaries is somewhat arbitrary and serves the purpose of illustration. In calculating R_2, we made use of the previous observations suggesting that Lipari-Szabo formalism is suitable for analysis of spin relaxation in solids:[3, 4]

$$R_2 = \frac{1}{20} c_{dip}^2 \{4J(0) + J(\omega_H - \omega_N) + 3J(\omega_N) + 3J(\omega_H) + 6J(\omega_H + \omega_N)\} + \frac{1}{20} c_{CSA}^2 \{4J(0) + 3J(\omega_N)\} \quad \text{(S1)}$$

where

$$J(\omega) = (1 - S^2)\frac{\tau}{1 + \omega^2 \tau^2}, \quad c_{dip} = -\frac{\mu_0}{4\pi}\frac{\gamma_H \gamma_N \hbar}{r_{NH}^3}, \quad \text{and} \quad c_{CSA} = \frac{2}{3}\gamma_N B_0 \Delta\sigma_N . \quad \text{(S2)}$$

The standard settings $r_{NH} = 1.02$ Å, $\Delta\sigma_N = -172$ ppm have been used in the computations, with static magnetic field strength $\gamma_H B_0 / 2\pi = 600$ MHz. The Redfield-theory expressions for spin relaxation are valid for the range of parameters covered, especially considering that only a fraction of the ^{1}H^N-^{15}N dipolar interaction is modulated by the internal protein motion. The time scale τ is sufficiently short so that the results do not need to be corrected for the effect of MAS.[5]

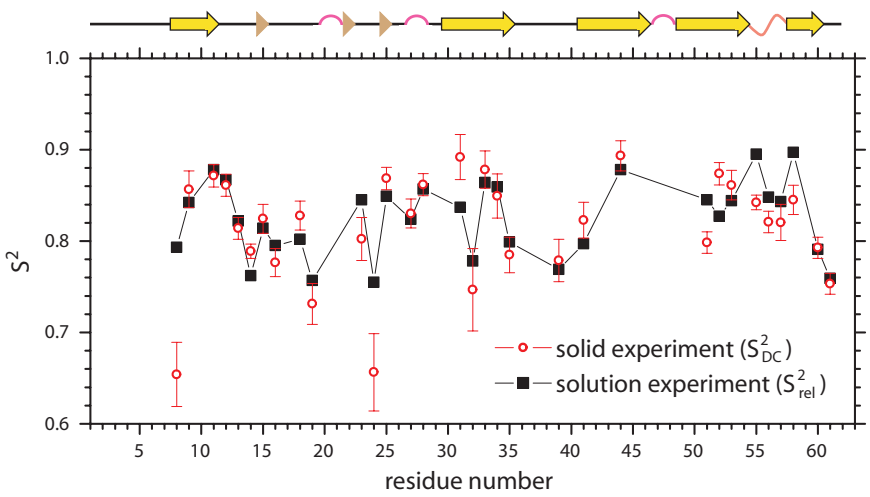

Figure S3. Experimentally determined order parameters in α-spectrin SH3. This plot is the equivalent of Fig.1 that additionally displays the estimated S^2_{DC} uncertainties. The error bars reflect the precision of the data, i.e. report on random errors; for discussion of small systematic errors see Chevelkov *et al.*[2] The secondary structure as determined by DSSP analysis[6] of 1U06 is: 8-11, 30-35, 41-46, 49-54 and 58-60 β-sheet, 55-57 3_{10}-helix, 20-21, 27-28, and 47-48 hydrogen-bonded turns, 15, 22, and 25 isolated β-bridges.

Residue number	S^2_{rel}	S^2_{DC}
2	(0.15)	-[a]
3	(0.19)	-[a]
4	(0.27)	-[a]
5	(0.27)	-[a]
6	(0.38)	-[a]
7	(0.62)	-[a]
8	0.79	0.65
9	0.84	0.86
10	0.87	-[b]
11	0.89	0.87
12	0.87	0.86
13	0.82	0.81
14	0.76	0.79
15	0.81	0.82
16	0.79	0.78
17	-[b]	-[b]
18	0.80	0.84
19	0.76	0.73
20	-[c]	-[c]
21	0.77	-[a]
22	0.87	-[b]
23	0.85	0.80
24	0.76	0.66
25	0.85	0.87
26	-[b]	0.84
27	0.82	0.83
28	0.86	0.86
29	0.89	0.87
30	-[b]	0.84
31	0.84	0.89
32	0.78	0.75

Residue number	S^2_{rel}	S^2_{DC}
33	0.86	0.88
34	0.86	0.85
35	0.80	0.78
36	0.82	-[a]
37	0.85	0.85
38	0.88	-[a]
39	0.77	0.79
40	0.81	0.84
41	0.80	0.82
42	0.82	0.86
43	0.83	-[b]
44	0.88	0.89
45	-[b]	0.84
46	-[b]	0.81
47	0.81	-[a]
48	-[a]	-[a]
49	-[b]	0.72
50	-[b]	0.71
51	0.85	0.80
52	0.83	0.87
53	0.84	0.86
54	-[c]	-[c]
55	0.90	0.84
56	0.85	0.82
57	0.84	0.82
58	0.90	0.84
59	-[b]	0.82
60	0.79	0.79
61	0.76	0.75
62	-[b]	0.35

Table S1. Experimentally measured relaxation-based and DC-based order parameters. The absent data are due to: (a) weak or missing peaks, (b) spectral overlaps, and (c) proline residues. The solution data from residues 2-7 have been analyzed using the extended, four-parameter version of Lipari-Szabo model.[7] All of these residues show substantial amount of motion on 1-2 ns time scale; reported in this table are the values of $S^2_{rel,f}S^2_{rel,s}$ (shown in brackets).

Order parameters and local dynamics.

1. *Isotropic local dynamics*

As a starting point in the discussion, let us assume that the local motion of an NH vector is characterized by a three-fold or higher symmetry. For instance, "diffusion in a cone" model that has axial symmetry (C_∞) fits this description.[8] It is straightforward to calculate the order parameters arising from this model. Considering relaxation experiments in solution, it is appropriate to use Eq. (1):

$$S^2 = (4\pi/5)\sum_{m=-2}^{2} < Y^*_{2m}(\theta,\varphi) >< Y_{2m}(\theta,\varphi) > \qquad \text{(S3)}$$

Here it is assumed that the tumbling of the molecule is isotropic, so that the directional angles of the NH vector (θ,φ) can be defined relative to an arbitrary molecular frame. Choosing a molecular frame such that its z axis lies along the axis of the cone, we obtain $< Y_{2m}(\theta,\varphi) >= 0$ for $m = \pm 1, \pm 2$. The order parameter is, therefore, reduced to $S^2 = (4\pi/5) < Y_{20}(\theta) >^2$. If local motion is much faster than the overall tumbling, then S^2 is equivalent to S^2_{rel} .

Considering dipolar coupling experiments in solids, it is convenient to start with the relevant Hamiltonian:

$$H_{dip} = c_{IS} 2 I_z S_z D^{L\leftarrow P}_{0,0}(0,\tilde{\theta},0) \qquad \text{(S4)}$$

where $c_{IS} = -(\mu_0/4\pi)\gamma_I\gamma_S\hbar/r^3_{IS}$, and $D^{L\leftarrow P}_{0,0}$ is the element of the second-rank Wigner matrix defined according to Haeberlen[9] that relates the principal axis frame P (z axis along the NH vector) to the laboratory frame L (z axis along the static magnetic field). To investigate the effect of the internal motion, H_{dip} needs to be rewritten as:

$$H_{dip} = c_{IS} 2 I_z S_z \sum_{p=-2}^{2} D_{p,0}^{L \leftarrow M}(0, \tilde{\tilde{\theta}}, 0) D_{0,p}^{M \leftarrow P}(\varphi, \theta, 0) \quad \text{(S5).}$$

Here we refer to the molecular frame M, which has its z axis along the axis of the cone. This frame is the same as used above in calculating S_{rel}^2, and the angles (θ, φ) have the same meaning. Assuming that the local motion is fast (in particular, faster than sample spinning in a MAS experiment), we can calculate the residual Hamiltonian that is partially averaged through the effect of the internal dynamics:

$$< H_{dip} >= c_{IS} 2 I_z S_z \sum_{p=-2}^{2} D_{p,0}^{L \leftarrow M}(0, \tilde{\tilde{\theta}}, 0) < D_{0,p}^{M \leftarrow P}(\varphi, \theta, 0) > \quad \text{(S6)}$$

As before, only the contribution with $p = 0$ survives, producing:

$$< H_{dip} >= c_{IS} 2 I_z S_z D_{0,0}^{L \leftarrow M}(0, \tilde{\tilde{\theta}}, 0) < D_{0,0}^{M \leftarrow P}(0, \theta, 0) > \quad \text{(S7)}$$

The above expression is equivalent to the original Hamiltonian Eq. (S4) aside from two aspects: (*i*) it implies that the NH vector is oriented along the axis of the cone of motion and (*ii*) it includes the factor $< D_{0,0}^{M \leftarrow P}(0, \theta, 0) >$ that effectively scales the interaction constant c_{IS}. This factor can be readily identified as DC order parameter and evaluated as follows: $S_{DC} =< D_{0,0}^{M \leftarrow P}(0, \theta, 0) >= (4\pi/5)^{1/2} < Y_{20}(\theta) >$. Thus, it becomes apparent that $S_{DC}^2 = S_{rel}^2$, consistent with the commonly made assumption.

Let us now consider the effect of internal dynamics on spin evolution under the conditions of CP recoupling in MAS experiment.[2] In principle, the existing results by Zilm and co-workers[10, 11] are applicable to this experiment if the constant c_{IS} is replaced with $c_{IS} S_{DC}$ (this follows from the fundamental similarity between Eq. (S4) and (S7)). Here we briefly illustrate the derivation of these results since it is relevant for the following discussion.

The Hamiltonian Eq. (S5) can be rewritten as:

$$H_{dip} = c_{IS} 2 I_z S_z \sum_{p,q=-2}^{2} D_{p,0}^{L \leftarrow R}(0, \beta_{MAS}, \omega_R t) D_{q,p}^{R \leftarrow M}(\alpha, \beta, \gamma) D_{0,q}^{M \leftarrow P}(\varphi, \theta, 0) \quad \text{(S8).}$$

Here R denotes the rotor frame, β_{MAS} is the magic angle, $\omega_R / 2\pi$ is the spinning speed, and (α, β, γ) define the transformation from the molecular frame to the rotor frame (in a polycrystalline sample, these angles are different for each individual crystallite). This result can be averaged with respect to the local motion (see above) and then rewritten using the explicit expressions for Wigner matrices:[9]

$$< H_{dip} >= c_{IS} 2 I_z S_z \sum_{p=-2}^{2} f_p \exp(ip\omega_R t) \quad \text{(S9).}$$

For the experiment with CP match at +1 (-1) spinning sideband,[2] the magnetization transfer is actuated by the coefficient f_1 (f_{-1}):[10]

$$| f_{\pm 1} |= \frac{\sqrt{2}}{4} S_{DC} | \sin 2\beta | \quad \text{(S10).}$$

Finally, the amplitude of the magnetization transfer associated with an individual crystallite is:[10]

$$S_x(t) \sim \sin^2\left(c_{IS} | f_{\pm 1} | \frac{t}{2} \right) \quad \text{(S11).}$$

In order to obtain the net signal, the result Eq. (S11) should be integrated over the surface of unit sphere (powder average). Note that the above treatment is rather basic. In particular, it neglects the effect of *rf* inhomogeneity and ^{15}N CSA interaction; it also makes no attempt to model the details of the actual pulse sequence.[2] Nevertheless, it is sufficient to form an idea about the role of local dynamics.

2. *Anisotropic local dynamics*

As an alternative scenario, let us now assume that the local motion lacks the C_n $(n \geq 3)$ symmetry. For example, let us examine a simple two-site jump model, where the NH vector hops between two (equally probable) orientations with the amplitude of the jump 2Φ. The relaxation order parameter for this model can be calculated in a straightforward fashion using Eq. (S3):[12]

$$S_{rel}^2 = 1 - (3/4) \sin^2 2\Phi \quad \text{(S12)}$$

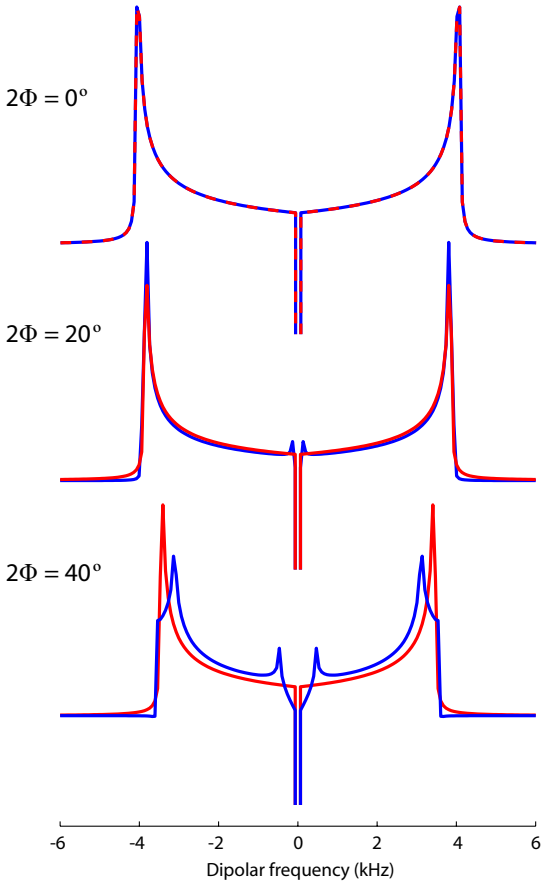

Figure S4. ^{15}N-^{1}H^{N} dipolar spectra simulated using the anisotropic model of local motion (Eqs. (S11) and (S14); blue traces) and the best fits of these simulated data using the isotropic model of local motion, (Eqs. (S11) and (S10); red traces). The fitting was performed by minimizing the *rms* deviation between the curves over the frequency interval from -6 to -0.5 kHz (0.5 to 6 kHz), which excludes the irrelevant spectral feature at zero frequency. The minimization was carried out using a grid search in a space of two parameters: S_{DC} and the overall signal amplitude.

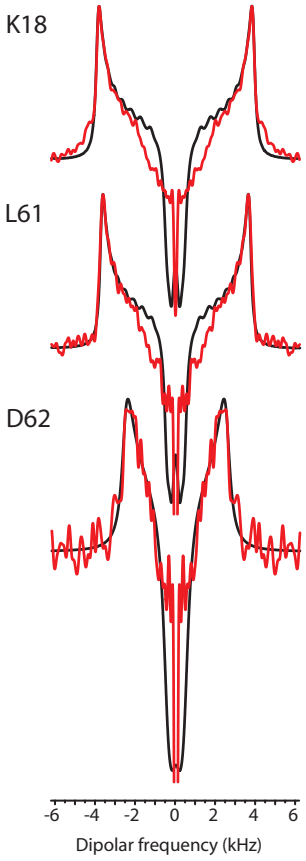

Figure S5. Experimental ^{15}N-^{1}H^{N} dipolar spectra of selected residues in α-spectrin SH3 domain (red traces) and best fits of these experimental data using the SIMPSON program[13] (black traces). Reproduced from Chevelkov *et al*.[2]

To analyze the solid-state experiment, it is convenient to cast the dipolar Hamiltonian in the following form:[3]

$$H_{dip}(\pm\Phi) = c_{IS}\, 2I_z S_z \sum_{p,q=-2}^{2} D_{p,0}^{L\leftarrow R}(0,\beta_{MAS},\omega_R t) D_{q,p}^{R\leftarrow M}(\alpha,\beta,\gamma) D_{0,q}^{M\leftarrow P}(\pm\Phi,\frac{\pi}{2},0) \qquad \text{(S13)}.$$

In this expression the molecular frame M is defined such that its z axis lies along the rotation axis of the two-site jump motion; the rotations by the amount $+\Phi$ and $-\Phi$ correspond to the two sampled NH orientations. The dynamic averaging, due to jumps between the two orientations, leads to $< H_{dip} >= (H_{dip}(\Phi) + H_{dip}(-\Phi))/2$. After some algebra, one obtains:

$$|f_{\pm 1}| = \frac{\sqrt{2}}{4} |\sin\beta| \sqrt{\cos^2\beta(1+\cos 2\gamma\cos 2\Phi)^2 + \sin^2 2\gamma\cos^2 2\Phi} \qquad \text{(S14)}$$

with Eq.(S11) describing the time evolution profile of an individual crystallite. To obtain the net signal, Eq. (S11) (complemented by Eq. (S14)) should be integrated over the surface of the unit sphere. The integration involves two angles, β and γ , instead of the single angle β in Eq. (S10). Indeed, there are two directional parameters in the present model: average orientation of the NH vector and the direction of the jump.

At this point we are prepared to investigate the potential impact of the motional anisotropy on the extracted values of S_{DC} . For this purpose, we simulated the DC time evolution profiles using Eq. (S14) and (S11) (the latter subject to powder averaging). The result was Fourier-transformed and the real part was retained, same as in our experimental procedure.[2] The resulting dipolar spectra are shown with blue lines in Fig. S4. The spectral pattern is obviously different from the generic shape (cf. top and bottom panels in Fig. S4). To understand why this is so, consider the NH vector that is oriented at a right angle to the rotor axis. If this vector jumps in the equatorial

plane then the effective dipolar coupling remains unchanged. Conversely, if the vector jumps in a meridional plane then the coupling is rescaled. This kind of behavior is responsible for the complex lineshapes observed in the simulations. The sensitivity of solid-state lineshapes to the details of local dynamics is a familiar phenomenon, especially well documented in the ^{2}H studies.[14]

The spectra simulated using the anisotropic model (two-site jumps) were subsequently fitted using the isotropic model (diffusion in a cone). The fits are represented by red traces in Fig. S4. As can be appreciated from the bottom panel in Fig. S4, the fitting criteria are open to discussion. In our simulations, we sought to minimize the *rms* deviation between the two spectral traces. Alternatively, one may seek to reproduce the distinctive spectral features, such as position of the 'horns'. With our fitting routine we were able to recover the S^2 values quite well. For example, for the jump amplitude $2\Phi = 20°$ the target order parameter is $S^2_{rel} = 0.91$ (see Eq. (S12)). At the same time, when the isotropic model is used to fit the simulated dipolar spectrum, the extracted order parameter is $S^2_{DC} = 0.90$. For the jump amplitude $2\Phi = 40°$ the corresponding numbers are 0.69 and 0.72.

In assessing the results in Fig. S4 one should keep in mind several considerations. First, the model where NH vector jumps by 40° almost certainly exaggerates the anisotropic character of motion. In reality, the motion of the NH vectors is usually fairly close to isotropic.[15] Second, as already mentioned, the simulations in Fig. S4 are simplistic in that they do not take into account ^{15}N CSA, *rf* inhomogeneity, proton relaxation, details of the actual pulse sequence, etc. When all these additional variables are included, the detection of motional anisotropy will likely become more difficult. Third, the experimental spectra have limited signal-to-noise ratio and resolution (illustrated in Fig. S5). This makes the detection of motional anisotropy even more problematic. Based on all these observations, we conclude that there is no support for use of the anisotropic model in the present study.

MD simulation protocol

The starting coordinates for the solid-state MD trajectory were obtained from the high-resolution crystallographic structure 1U06.[16] This structure misses six N-terminal residues and one C-terminal residue. As discussed in the text, the N-terminal region is significantly disordered in the crystalline state and undergoes a nanosecond time scale conformational exchange. Given that the terminal residues are absent from the crystallographic structures (as well as solid-state NMR structure[17]), it is necessary to model these residues while taking into consideration the effects of crystal packing.

Toward this goal, we produced 150 structural models based on 1U06 geometry, where the terminal segments were initially generated in a form of random coil[18] and appended to the body of the protein. The resulting constructs were packed into a unit cell (space group $P2_12_12_1$, four protein molecules per cell). The dimension of the unit cell, $34.47 \times 42.48 \times 50.80$ Å , were taken from a room-temperature crystallographic structure 2NUZ. The cells were subsequently hydrated using the standard facilities of the CHARMM program.[19]

As a next step, the coordinates of the terminal residues were optimized for each model using the protocol adapted from Sali et al.[20] To emulate crystal lattice environment, periodic boundary conditions have been applied at the faces of the unit cell. All heavy atoms in protein molecules, except those in six N-terminal residues and one C-terminal residue, have been fixed. The optimization procedure, implemented in CHARMM (version 32b2, CHARMM22 force field), begins with 500 steps of steepest descent minimization, followed by 500 steps of adopted basis Newton-Raphson minimization. The system is then heated from 100 to 1000 K with a step of 225 K and subsequently cooled back to 100 K (integration time step 1 fs, other parameters as described by Xue et al.[21]; total duration of the heating and cooling stages is 4 and 12 ps, respectively). Finally, the model is subjected to 200 rounds of Powell minimization.

The 150 optimized models were ranked according to energy and the lowest-energy model was chosen as a starting point for the MD production run.* The described MD setup rigorously accounts for all crystal contacts formed by α-spectrin SH3 in the orthorhombic cell. In the selected lowest-energy model, each protein molecule makes contacts with 6 neighboring molecules and 35% of the solvent accessible surface area is occupied by crystal contacts.

The MD simulation protocol was the same as used previously to generate the 30-ns trajectory of α-spectrin SH3 in solution.[7, 21] The only difference concerns the definition of the water box and the associated periodic boundary conditions (PBCs). In the case of the solid-state simulation, the PBCs are intended to recreate the crystal lattice environment, including multiple crystal contacts. In solution, on the other hand, the water box is constructed to ensure that the protein is surrounded by a sufficiently thick water shell which prevents direct contacts between the protein and its PBC image.

The 50-ns solid-state MD trajectory was recorded in ca. 2 months using one GNU/Linux workstations equipped with a pair of 3-GHz dual-core Xeon processors. Given that the simulation involves 4 protein molecules contained in the crystal unit cell, the actual statistics is better than suggested by the nominal length of the trajectory. The convergence can be judged from the spread in the simulated S^2_{DC} values (pink shaded area in Fig. 2 of the text). The trajectories were processed as described previously.[21] An attempt to eliminate small-amplitude reorientational motions (i.e. 'rocking' of protein molecules in the crystal lattice) had virtually no impact on the extracted order parameters. In the final protocol the simulated solid-state data were treated as is, with no attempt to eliminate any motional modes.

The previously described solution trajectory[7, 21] has been extended to the total length of 50 ns in order to match the length of the solid-state trajectory.

* As a control, we have chosen another low-energy model, showing a different conformation of the N-terminus, and recorded a 30-ns trajectory starting with this alternative model. The results proved to be similar and are not reported in this paper.

References

(1) Linser, R.; Chevelkov, V.; Diehl, A.; Reif, B. J. Magn. Reson. 2007, 189, 209.
(2) Chevelkov, V.; Fink, U.; Reif, B. J. Am. Chem. Soc. 2009, 131, 14018.
(3) Skrynnikov, N. R. Magn. Reson. Chem. 2007, 45, S161.
(4) Agarwal, V.; Xue, Y.; Reif, B.; Skrynnikov, N. R. J. Am. Chem. Soc. 2008, 130, 16611.
(5) Farès, C.; Qian, J.; Davis, J. H. J. Chem. Phys. 2005, 122.
(6) Kabsch, W.; Sander, C. Biopolymers 1983, 22, 2577.
(7) Chevelkov, V.; Zhuravleva, A. V.; Xue, Y.; Reif, B.; Skrynnikov, N. R. J. Am. Chem. Soc. 2007, 129, 12594.
(8) Richarz, R.; Nagayama, K.; Wuthrich, K. Biochemistry 1980, 19, 5189.
(9) Haeberlen, U., High resolution NMR in solids. Selective Averaging. In Advances in Magnetic Resonance, Suppl. 1, Waugh, J. S., Ed., Academic Press: New York, 1976.
(10) Wu, X. L.; Zilm, K. W. J. Magn. Reson. Ser. A 1993, 104, 154.
(11) Paulson, E. K.; Martin, R. W.; Zilm, K. W. J. Magn. Reson. 2004, 171, 314.
(12) Daragan, V. A.; Mayo, K. H. J. Magn. Reson. Ser. B 1995, 107, 274.
(13) Bak, M.; Rasmussen, J. T.; Nielsen, N. C. J. Magn. Reson. 2000, 147, 296.
(14) Spiess, H. W. Adv Polym Sci 1985, 66, 23; Hoatson, G. L.; Vold, R. L., 2H NMR spectroscopy of solids and liquid crystals. In NMR Basic Principles and Progress, Diehl, P.; Fluck, E.; Gunther, H.; Kosfield, R.; Seelig, J., Ed., Springer-Verlag: Berlin, 1994; 32, 1; Hologne, M.; Faelber, K.; Diehl, A.; Reif, B. J. Am. Chem. Soc. 2005, 127, 11208.
(15) Lienin, S. F.; Bremi, T.; Brutscher, B.; Bruschweiler, R.; Ernst, R. R. J. Am. Chem. Soc. 1998, 120, 9870; Yao, L.; Vögeli, B.; Torchia, D. A.; Bax, A. J. Phys. Chem. B 2008, 112, 6045.
(16) Chevelkov, V.; Faelber, K.; Diehl, A.; Heinemann, U.; Oschkinat, H.; Reif, B. J. Biomol. NMR 2005, 31, 295.
(17) Castellani, F.; van Rossum, B.; Diehl, A.; Schubert, M.; Rehbein, K.; Oschkinat, H. Nature 2002, 420, 98.
(18) Feldman, H. J.; Hogue, C. W. V. Proteins: Struct. Funct. Genet. 2000, 39, 112.
(19) Brooks, B. R.; Brooks, C. L.; Mackerell, A. D.; Nilsson, L.; Petrella, R. J.; Roux, B.; Won, Y.; Archontis, G.; Bartels, C.; Boresch, S.; Caflisch, A.; Caves, L.; Cui, Q.; Dinner, A. R.; Feig, M.; Fischer, S.; Gao, J.; Hodoscek, M.; Im, W.; Kuczera, K.; Lazaridis, T.; Ma, J.; Ovchinnikov, V.; Paci, E.; Pastor, R. W.; Post, C. B.; Pu, J. Z.; Schaefer, M.; Tidor, B.; Venable, R. M.; Woodcock, H. L.; Wu, X.; Yang, W.; York, D. M.; Karplus, M. J. Comput. Chem. 2009, 30, 1545.
(20) Fiser, A.; Do, R. K. G.; Sali, A. Protein Sci 2000, 9, 1753.
(21) Xue, Y.; Pavlova, M. S.; Ryabov, Y. E.; Reif, B.; Skrynnikov, N. R. J. Am. Chem. Soc. 2007, 129, 6827.